Available online at www.sciencedirect.com

SciVerse ScienceDirect

Ceramics International 39 (2013) 2567–2573

CERAMICS INTERNATIONAL

www.elsevier.com/locate/ceramint

# PEG-directed microwave-assisted hydrothermal synthesis of spherical α-$Ni(OH)_2$ and NiO architectures

Zhenfeng Zhu, Yanbin Zhang*, Yanli Zhang, Hui Liu, Chunkui Zhu, Yingfeng Wu

*School of Materials Science and Engineering, Shaanxi University of Science and Technology, Xi'an 710021, PR China*

Received 4 July 2012; received in revised form 5 September 2012; accepted 5 September 2012
Available online 13 September 2012

**Abstract**

Spherical α-$Ni(OH)_2$ architectures were synthesized by the microwave-assisted hydrothermal technique using PEG-6000 as the surfactant. NiO architectures with similar morphology were obtained by a simple thermal decomposition process of the precursor α-$Ni(OH)_2$ at 400 °C for 2 h and were confirmed by the X-ray diffraction (XRD) analysis. Scanning electron microscopy (SEM) revealed that the synthesized spherical α-$Ni(OH)_2$ and NiO architectures were composed of stacked lamellar sheets and transmission electron microscopy (TEM) showed that the α-$Ni(OH)_2$ and NiO architectures were polycrystalline. The effect of the PEG-6000 concentration on particle size was investigated and it was found that the average particle size of α-$Ni(OH)_2$ architectures decreased from 4.689 μm at $C_{PEG}=2$ mmol $L^{-1}$ to 3.907 μm at $C_{PEG}=4$ mmol $L^{-1}$, and the corresponding average particle size of NiO decreased from 2.818 μm to 2.492 μm. The optical absorption band gap of NiO architectures was determined to be about 2.7–3.0 eV by UV–vis spectroscopy.


*Keywords:* B. X-ray methods; C. Optical properties; D. Transition metal oxides

## 1. Introduction

Nickel hydroxide ($Ni(OH)_2$), as one of the most important transition metal hydroxides, has received increasing attention due to its extensive applications, especially as a material in the positive electrodes of rechargeable alkaline Ni-based batteries [1–3]. So far, nickel hydroxide with various morphologies have been synthesized including nanoplates [4], hollow spheres [5], flowerlike [6], ribbonlike and boardlike [7] structures. Besides, Nickel oxide (NiO) demonstrates excellent properties such as catalytic [8], magnetic [9], electrochromic [10], optical and electrochemical [11] properties. Furthermore, nickel oxide can be used as a kind of transparent p-type semiconductor [12] and is being studied for applications in smart windows, electrochemical supercapacitors [13,14] and dye-sensitized photocathodes [15]. NiO also has the benefit of conveniently being prepared by thermal decomposition of its precursors [16].

Microwave-assisted hydrothermal synthesis has some advantages such as short heating time, homogeneous thermal transmission, and the ability to produce narrow particles with high purity [17–19]. Vanetsev et al. have studied the synthesis of spherical oxide particles in microwave hydrolysis [18]. Xu et al. have successfully synthesized 3D flowerlike α-nickel hydroxide with enhanced electrochemical activity by the microwave-assisted hydrothermal method [19]. However, few investigations were concerned on the effect of the PEG surfactant on the synthesis of the α-$Ni(OH)_2$ and NiO architectures. Therefore, the aim of this study is to synthesize relatively small α-$Ni(OH)_2$ and NiO architectures via a simple microwave-assisted hydrothermal synthesis method in a short time and investigate the effect of the PEG-6000 on the synthesis of the α-$Ni(OH)_2$ and NiO architectures.

Herein, we reported a microwave-assisted hydrothermal method to synthesize spherical α-$Ni(OH)_2$ architectures via the reaction between $Ni(NO_3)_2 \cdot 6H_2O$ and urea with the addition of the polymer PEG-6000. These α-$Ni(OH)_2$ architectures then underwent thermal decomposition to yield NiO architectures that remained the spherical morphology. Finally, the optical and electrochemical properties of the NiO samples were investigated.

*Corresponding author. Tel./fax: +86 29 86168331.
*E-mail address:* zhang.yanbin@163.com (Y. Zhang).

0272-8842/$ - see front matter 
http://dx.doi.org/10.1016/j.ceramint.2012.09.017

## 2. Experimental section

### 2.1. Synthesis of α-Ni(OH)$_2$ and NiO architectures

Spherical α-Ni(OH)$_2$ architectures were prepared by a microwave hydrothermal process. All of the raw materials were of analytical grade reagents and were used without further purification. In the synthesis process, 0.9 g of PEG-6000 surfactant (Tianjin Fu Chen Chemical Reagents Factory) was dissolved in 50 mL deionized water to form a transparent solution. Then $Ni(NO_3)_2 \cdot 6H_2O$ (0.1 mol $L^{-1}$, Sinopharm Chemical Reagent Co., Ltd.) was added with vigorous stirring, followed by the addition of $CO(NH_2)_2$ solution (0.5 mol $L^{-1}$, Tianjin Fu Chen Chemical Reagents Factory), also with vigorous stirring to form a clear blue solution. The molar ratio of $Ni(NO_3)_2 \cdot 6H_2O$ and $CO(NH_2)_2$ was 1:1. The solution was then transferred to a 100 mL (filling ratio = 50%) Teflon-lined autoclave and treated at 160 °C for specific 30 min under the temperature-controlled mode in a MDS-8 microwave hydrothermal system. After the reaction was terminated, the product was allowed to cool to room temperature. The resulting pale green slurry was rinsed and filtered with deionized water and absolute ethanol (Tianjin Hedong Red Cliff Chemical Reagent Factory) several times to remove soluble impurities. The precipitate was dried at 80 °C in a vacuum oven for 12 h to get the sample of α-Ni(OH)$_2$. To obtain the NiO architectures, the as-prepared α-Ni(OH)$_2$ precursors were calcined at 400 °C in air for 2 h.

### 2.2. Characterization

The as-prepared samples were characterized by X-ray powder diffraction (XRD) with a Rigaku D/max 2550 X-ray diffractometer with a high-intensity Cu Kα radiation ($\lambda = 1.5417$ Å) and a graphite monochromator. The step size and dwell time were 0.02° and 0.2 s, respectively. The microstructures of the sample were analyzed by scanning electron microscopy (SEM; JEOL JSM-6360, Japan) with an accelerating voltage of 5.0 kV. The transmission electron microscopy (TEM) micrographs and selected-area electron diffraction (SAED) patterns were taken with a JEOM JSM-3010 field emission transmission electron microscope with an accelerating voltage of 200 kV. TEM samples were ultrasonically dispersed in ethanol, and then a drop of the liquid was placed on a thin amorphous carbon film supported by a copper grid. The particle sizes of the samples were measured by a Nano-ZS (Malvern Zetasizer, UK) after the samples were dispersed in the ethanol to form a stable suspension. The absorption spectra were measured with a UV–vis spectrophotometer (Lambda 950, PerkinElmer) in the wavelength range of 200–800 nm. The samples prepared for the UV–vis spectrophotometer measurement were in the powder form.

## 3. Results and discussion

### 3.1. XRD analysis

As shown in Fig. 1, X-ray diffraction (XRD) was used to study the phase purity of the obtained nickel hydroxide. The peaks at $2\theta = 12.2°$ and 24.8° corresponded to the (001) and (002) planes, respectively, with a slight shift (JCPDS, 02–1112). These shifts were attributed to the extent and type of the water molecule in the α-Ni(OH)$_2$ lattice. The peak at $2\theta = 33.4°$ was due to the diffraction peak of $\alpha\text{-}Ni(OH)_2 \cdot 0.75H_2O$, which can be readily indexed as (101) crystal plane. In addition, the peak at $2\theta = 59.8°$ was associated with the diffraction peak of $\alpha\text{-}3Ni(OH)_2 \cdot 2H_2O$, which can be readily indexed as (101) crystal plane. No peaks of other substances were observed in the XRD patterns. Notably, the intensity of all the peaks decreased when the concentration of PEG-6000 increased from 2 to 4 mmol $L^{-1}$, which indicated that the crystallinity of nickel hydroxide was lower with a higher concentration of PEG-6000.

Fig. 2 shows the XRD patterns of the NiO architectures synthesized under different conditions. The diffraction peaks corresponding to cubic NiO appearing at $2\theta = 37.24°$, 43.26°, 62.76°, 75.48° and 79.32° can be readily indexed as the (111), (200), (220), (311) and (222) crystal planes, respectively. All of these diffraction peaks, not only in the peak positions but also in their relative intensity, were in accordance with the standard spectrum (JCPDS, 78–0643).

### 3.2. FE-SEM analysis

The surface morphological study of the α-Ni(OH)$_2$ architectures using FE-SEM is shown in Fig. 3. It can be found that the morphology of the α-Ni(OH)$_2$ architectures

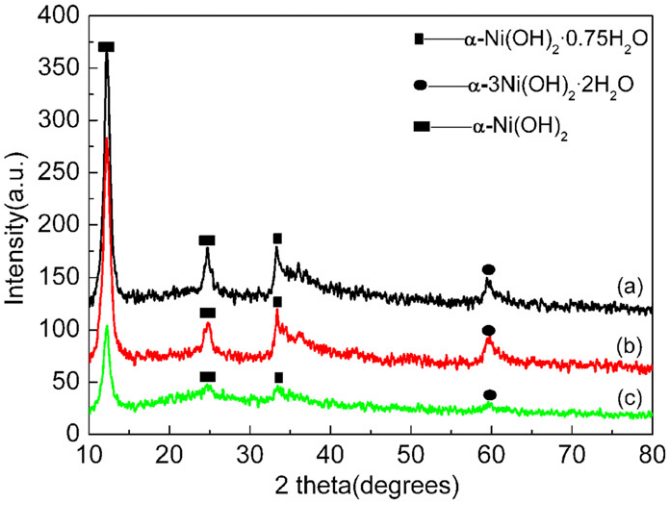


Fig. 1. XRD patterns of the α-Ni(OH)$_2$ architectures synthesized at different conditions: (a) $C_{PEG} = 2$ mmol $L^{-1}$, (b) $C_{PEG} = 3$ mmol $L^{-1}$ and (c) $C_{PEG} = 4$ mmol $L^{-1}$.

were spherical with a stacked layered structure. Fig. 3a, b and c shows the overviews of the spherical α-Ni(OH)$_2$ architectures synthesized with $C_{PEG}$=2, 3 and 4 mmol L$^{-1}$, respectively. The corresponding diameters of the samples decreased from about 5.0 to 2.0 μm. It can be seen that the diameter of the samples was in size range of 2.0–5.0 μm (Fig. 4). Fig. 3d, e, f are the FE-SEM images of three single α-Ni(OH)$_2$ microspheres synthesized with $C_{PEG}$=2, 3 and 4 mmol L$^{-1}$, respectively. It can be found that the α-Ni(OH)$_2$ microspheres were comprised of densely packed irregular sheets. The diameters of the three single α-Ni(OH)$_2$ microspheres decreased from about 5.0 to 2.0 μm in turn.

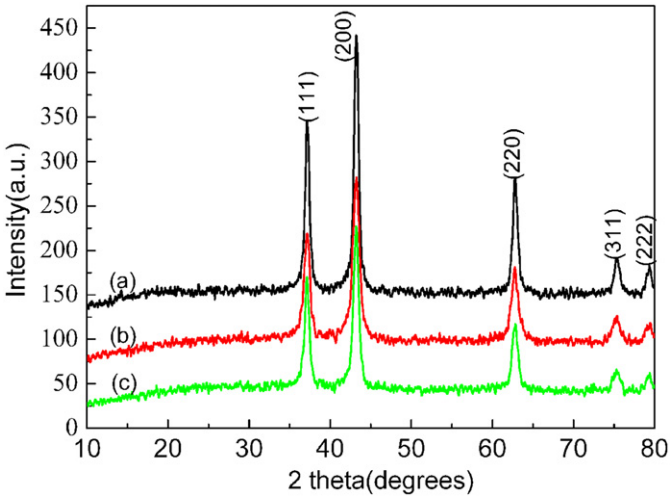


Fig. 2. XRD patterns of the NiO architectures synthesized at different conditions: (a) $C_{PEG}$=2 mmol L$^{-1}$, (b) $C_{PEG}$=3 mmol L$^{-1}$ and (c) $C_{PEG}$=4 mmol L$^{-1}$.

The average particle size of α-Ni(OH)$_2$ architectures was found to be decreasing with the increasing concentration of the PEG-6000 (Fig. 4a, b, c) and was plotted in Fig. 4d. The average particle size of the α-Ni(OH)$_2$ architectures were found to be 4.689 μm, 4.185 μm and 3.907 μm synthesized with $C_{PEG}$=2, 3 and 4 mmol L$^{-1}$, respectively.

Fig. 5 shows the FE-SEM images of the as-synthesized products. It was clear that in all cases (Fig. 5a, b and c), the NiO architectures with the spherical morphology were successfully prepared. To investigate the effect of surfactant's concentration on the particle size distribution, the particle size was indentified in each case (Fig. 6a, b and c). The diameter of the sample (a) synthesized with the $C_{PEG}$=2 mmol L$^{-1}$ was in size range of 1.0–6.0 μm (Fig. 6a). Fig. 5b was an overview of the spherical NiO architectures synthesized with the $C_{PEG}$=3 mmol L$^{-1}$. It can be found that the diameter of the samples was uniform in size range of 0.5–4.0 μm (Fig. 6b). Fig. 5c demonstrates the FE-SEM micrographs of the NiO architectures synthesized with $C_{PEG}$=4 mmol L$^{-1}$. It can be found that the samples were built up of numerous aggregated particles. The diameters of these particles were in the range from 1.0 to 3.6 μm (Fig. 6c). Fig. 5d, e and f are the FE-SEM micrographs of three single NiO microspheres. The diameter of the three single NiO microspheres decreased from about 3.5 μm to 1.5 μm in turn. The average particle size of NiO architectures was found to be decreasing with increase in the concentration of PEG-6000 and is plotted in Fig. 6d. The measured average nanoparticle size for the samples were 2.818 μm, 2.681 μm and 2.492 μm synthesized with $C_{PEG}$=2, 3 and 4 mmol L$^{-1}$, respectively. It also can be found that the gap between the average particle size of α-Ni(OH)$_2$ and NiO were 1.871 μm, 1.504 μm and 1.415 μm in turn, respectively.

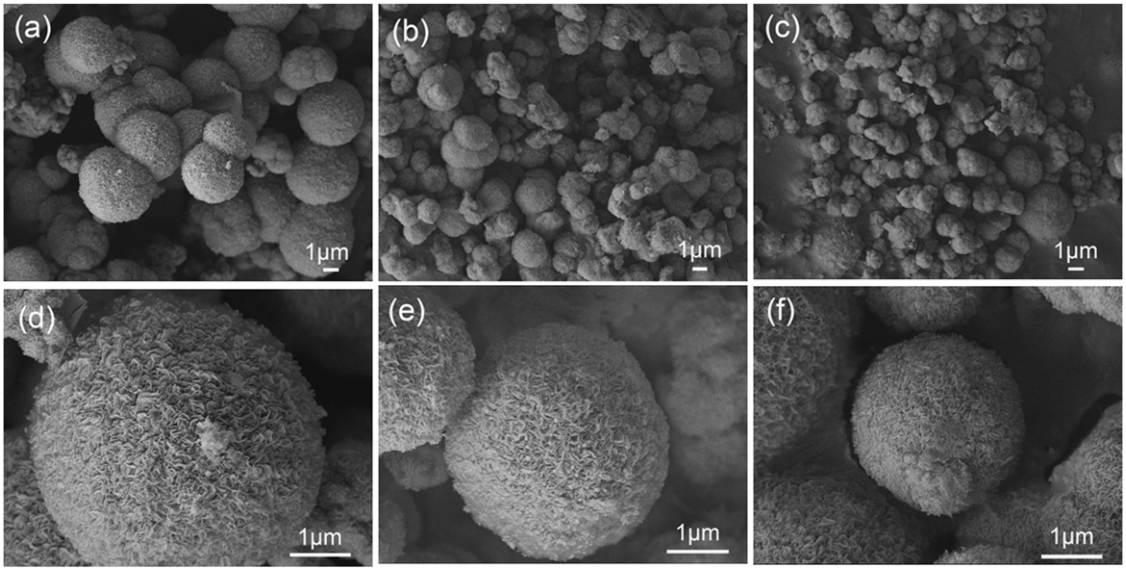


Fig. 3. FE-SEM of the α-Ni(OH)$_2$ architectures synthesized at different conditions: (a) $C_{PEG}$=2 mmol L$^{-1}$, (b) $C_{PEG}$=3 mmol L$^{-1}$ and (c) $C_{PEG}$=4 mmol L$^{-1}$; FE-SEM of the single α-Ni(OH)$_2$ microspheres synthesized at different conditions: (d) $C_{PEG}$=2 mmol L$^{-1}$, (e) $C_{PEG}$=3 mmol L$^{-1}$ and (f) $C_{PEG}$=4 mmol L$^{-1}$.

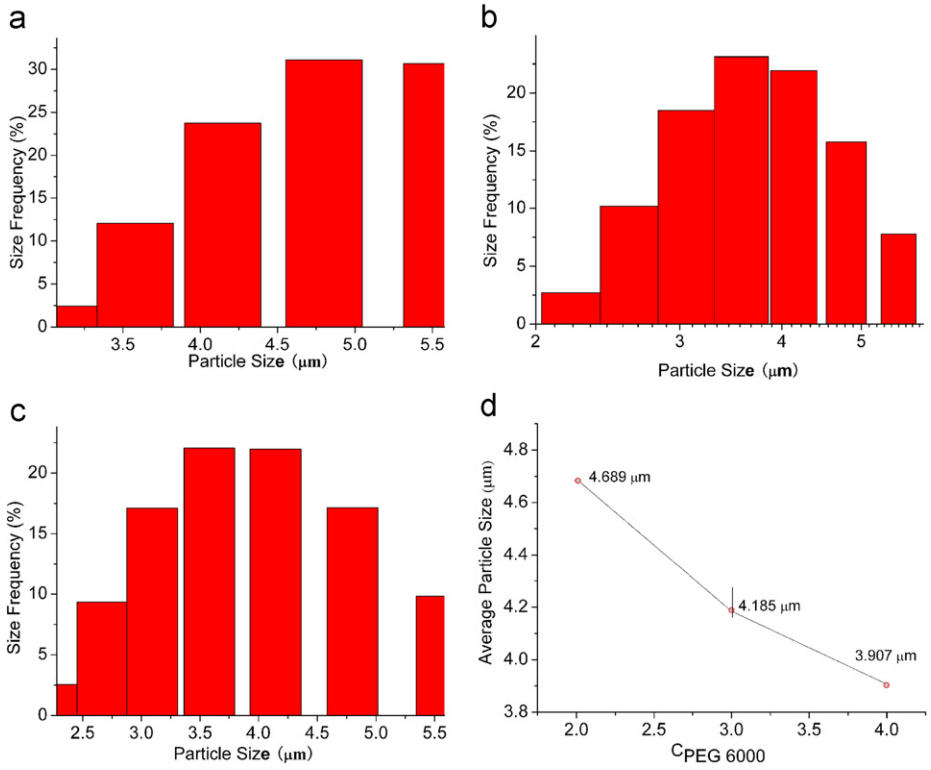


Fig. 4. Particle size distributions of α-$Ni(OH)_2$ architectures with different concentrations of PEG-6000: (a) $C_{PEG}=2$ mmol $L^{-1}$, (b) $C_{PEG}=3$ mmol $L^{-1}$, (c) $C_{PEG}=4$ mmol $L^{-1}$, and (d) average grain size (μm) of α-$Ni(OH)_2$ architectures as a function of the concentration of PEG-6000.

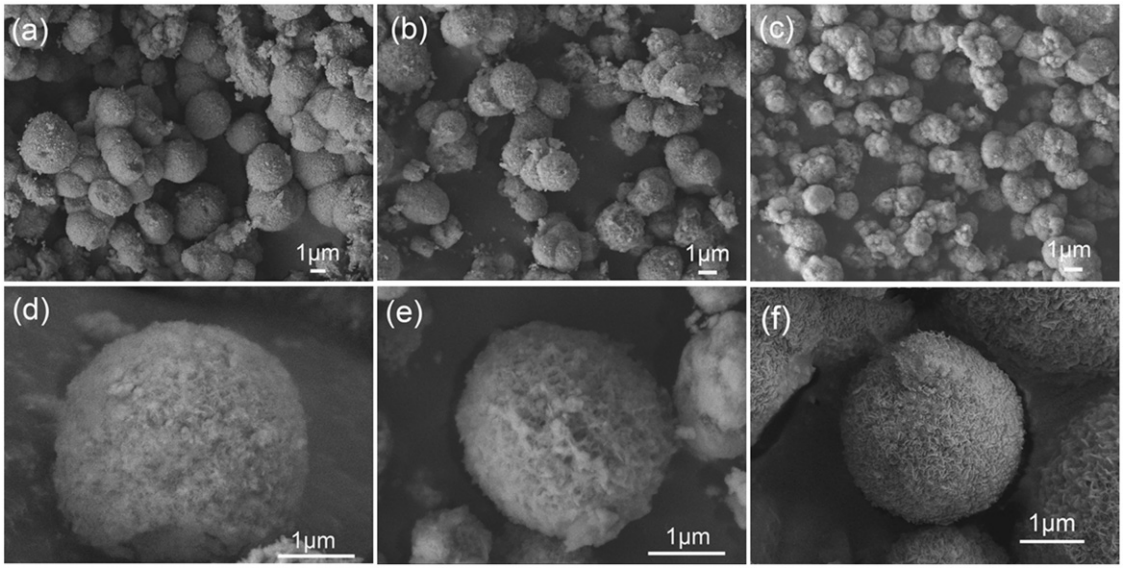


Fig. 5. FE-SEM images of calcined NiO architectures synthesized at different conditions: (a) $C_{PEG}=2$ mmol $L^{-1}$, (b) $C_{PEG}=3$ mmol $L^{-1}$ and (c) $C_{PEG}=4$ mmol $L^{-1}$; FE-SEM images of the single NiO microspheres synthesized at different conditions: (d) $C_{PEG}=2$ mmol $L^{-1}$, (e) $C_{PEG}=3$ mmol $L^{-1}$ and (f) $C_{PEG}=4$ mmol $L^{-1}$.

These changes in the size of nanoparticles can be attributed to the effect of the PEG-6000 surfactant on the synthesis of the α-$Ni(OH)_2$. During the synthesis of $Ni(OH)_2$ particles, the structure and morphology were determined by factors such as choice of surfactants, nickel salts and temperature of synthesis. Nickel salt is stable in neutral solution (pH∼7). The structure of the surfactant plays an important role in determining the morphology of the synthesized nanoparticles. PEG-6000 is a type of nonionic surfactant, whose molecular formula is $H(OCH_2-CH_2)_nOH$. The particles size decreased with the increasing concentration of PEG-6000, which was attributed to the PEG suppressing

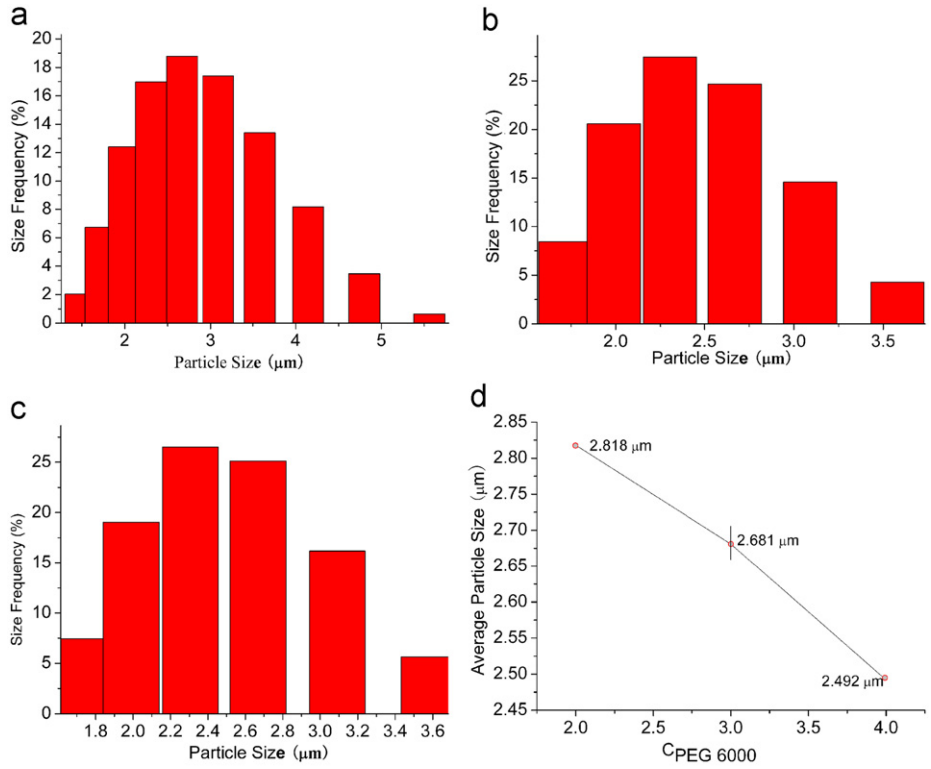


Fig. 6. Particle size distributions of NiO architectures with different concentrations of PEG-6000: (a) $C_{PEG}=2$ mmol $L^{-1}$, (b) $C_{PEG}=3$ mmol $L^{-1}$, (c) $C_{PEG}=4$ mmol $L^{-1}$ and (d) average grain size (μm) of NiO architectures as a function of the concentration of PEG-6000.

the growth rate of the particles by coating on the surface of the newly formed $Ni(OH)_2$ particles. The repellent action between the particles increased with the existence of PEG-6000. Garbuzenko et al. [20] elucidated that liposome size and specific turbidity decreased with the increase in temperature and PEG–DSPE mol%.

### 3.3. TEM analysis

TEM and SAED analysis were carried out on the α-$Ni(OH)_2$ and calcined NiO architectures to observe the individual size, shape and crystallinity of the samples. It can be seen in Fig. 7a that the as-synthesized α-$Ni(OH)_2$ samples exhibited a microsphere structure with a diameter range of 2.0–4.0 μm, which was consistent to the FE-SEM observations. Fig. 7b is the corresponding selected area diffraction (SAED) patterns of the sample. SAED patterns recorded on different particles were essentially the same and the diffraction rings matched the XRD peaks very well, which indicated that the microspheres were polycrystalline. As shown in Fig. 7c, the calcined NiO architectures also exhibited a microsphere structure with a diameter about 2.5 μm. The corresponding SAED patterns in Fig. 7d also confirmed that the NiO architectures had a face-centered cubic (FCC) structure, which was in line with the above XRD results.

### 3.4. Optical properties

Fig. 8 shows the UV–vis spectra of the calcined NiO architectures synthesized with different conditions. As shown in Fig. 8, a strong absorption in the UV region was observed at wavelengths about 370 nm, which was due to the band gap absorption in NiO [21]. Meanwhile, a strong absorption was observed at 393 nm in the visible region, which was attributed to intra-3d transition of $Ni^{2+}$ in the cubic structure of NiO [22,23]. The optical band gap, $E_g$, was calculated based on the data from the optical absorption spectra with the following equation:

$$(Ahv)^n = B(hv-E_g) \quad (1)$$

where $hv$ is the photon energy, $A$ is absorbance, $B$ is a constant relative to the material and $n$ is either two for direct transition or 1/2 for an indirect transition. Hence, the optical band gap for the absorption peaks can be obtained by extrapolating the linear portion of the $(Ahv)^n$–$hv$ curve to zero.

Fig. 9 shows the $(Ahv)^2$ versus $hv$ curve for the calcined NiO architectures synthesized at different conditions: (A) $C_{PEG}=2$ mmol $L^{-1}$, (B) $C_{PEG}=3$ mmol $L^{-1}$, (C) $C_{PEG}=4$ mmol $L^{-1}$. The band gap of the as-synthesized NiO samples was determined to be 2.7–3.0 eV by the extrapolation of the above equation, which demonstrated an obvious red-shift compared with that of the bulk NiO (4.0 eV) [24]. Theoretically, a generally received opinion

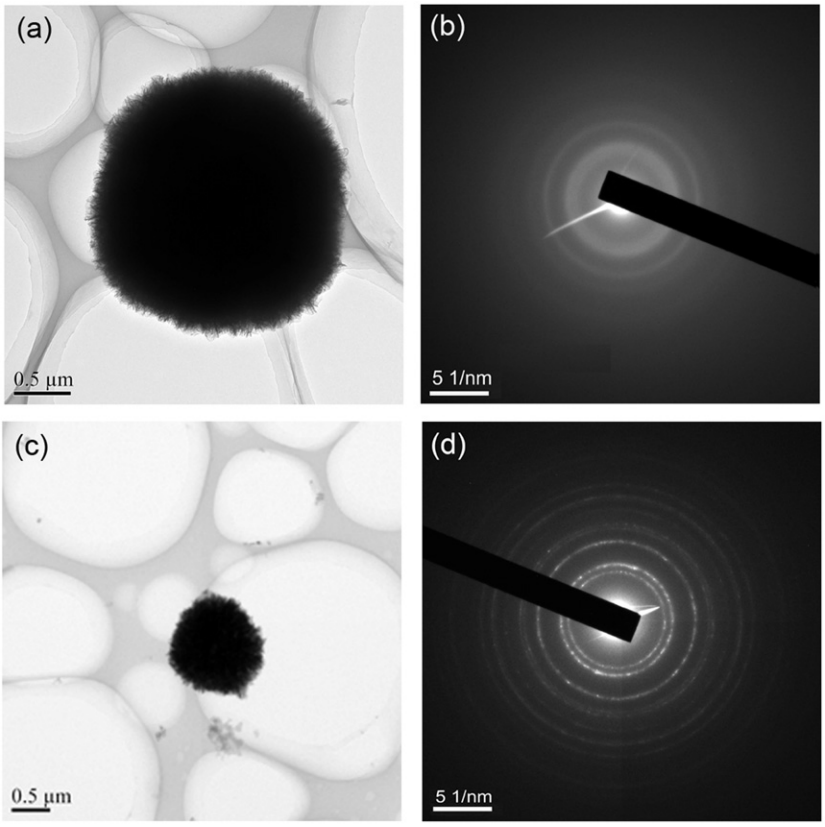


Fig. 7. TEM and SAED images of α-Ni(OH)$_2$ (a, b) and NiO (c, d) architectures synthesized at $C_{PEG}$=2 mmol L$^{-1}$.

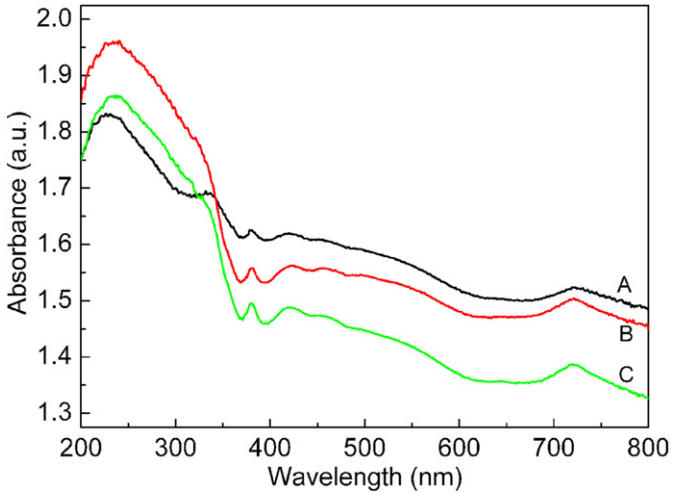


Fig. 8. UV–vis absorption spectrum of calcined NiO architectures synthesized at different conditions: (A) $C_{PEG}$=2 mmol L$^{-1}$, (B) $C_{PEG}$= 3 mmol L$^{-1}$ and (C) $C_{PEG}$=4 mmol L$^{-1}$.

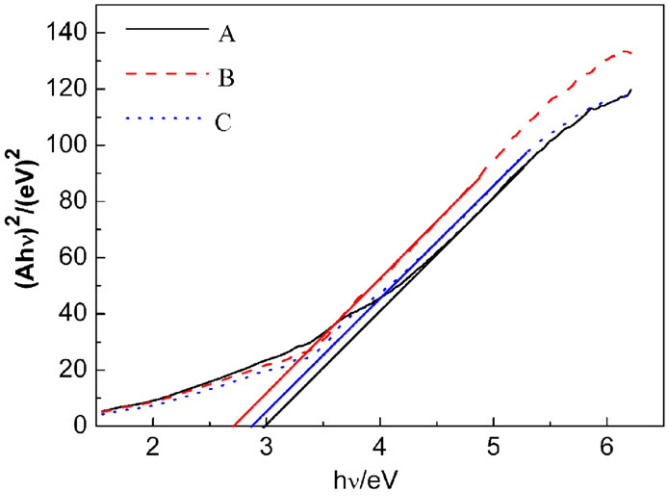


Fig. 9. The $(Ahv)^2$ versus $hv$ curve for the calcined NiO architectures synthesized at different conditions: (A) $C_{PEG}$=2 mmol L$^{-1}$, (B) $C_{PEG}$= 3 mmol L$^{-1}$ and (C) $C_{PEG}$=4 mmol L$^{-1}$.

was that the ubiquitous red shift might arise from quantum size effect. No linear relation was found for $n=1/2$, indicating that the as-prepared NiO architectures were semiconducting with direct transition at this energy. In the long-wavelength side, the long tail of the absorption was probably due to the scattered radiation of nickel oxide clusters of nanoparticles.

## 4. Conclusions

α-Ni(OH)$_2$ architectures were synthesized by the microwave-assisted hydrothermal technique using PEG-6000 as the surfactant. The synthesized α-Ni(OH)$_2$ architectures were found to be polycrystalline and spherical in shape. The shape consistent NiO architectures were

obtained by thermal decomposition of α-$Ni(OH)_2$ precursors. By increasing the concentration of PEG-6000, the size of architectures decreased. α-$Ni(OH)_2$ architectures with the average diameter of 4.689 μm, 4.185 μm and 3.907 μm were obtained when synthesized with the $C_{PEG}=2$, 3 and 4 mmol $L^{-1}$, respectively. NiO architectures with the average diameter of 2.818 μm, 2.681 μm and 2.492 μm were obtained when synthesized with the $C_{PEG}=2$, 3 and 4 mmol $L^{-1}$, respectively. The experimental observation was supported by SEM and TEM analyses. The optical absorption band gap of NiO architectures is about 2.7–3.0 eV. This method may be extended to synthesize other hierarchical nanostructures in the future.

## Acknowledgments

This work was financially supported by the National Science Foundation of China (No. 50772064), the Special Found from Shaanxi Provincial Department of Education (09JK355), and the Postgraduate Innovation Fund of Shaanxi University of Science and Technology.

## References

[1] H.M. French, M.J. Henderson, A.R. Hillman, et al., Ion and solvent transfer discrimination at a nickel hydroxide film exposed to LiOH by combined electrochemical quartz crystal microbalance (EQCM) and probe beam deflection (PBD) techniques, Journal of Electroanalytical Chemistry 500 (2001) 192–207.

[2] G.J.de A.A. Soler-Illia, M. Jobbagy, A. Regazzoni, et al., Synthesis of nickel hydroxide by homogeneous alkalinization. precipitation mechanism, Chemistry of Materials 11 (1999) 3140–3146.

[3] Y. Luo, G. Li, G. Duan, et al., One-step synthesis of spherical α-$Ni(OH)_2$ nanoarchitectures, Nanotechnology 17 (2006) 4278–4283.

[4] J. Zhu, Z. Gui, Y. Ding, et al., A facile route to oriented nickel hydroxide nanocolumns and porous nickel oxide, Journal of Physical Chemistry C 111 (2007) 5622–5627.

[5] G. Duan, W. Cai, Y. Luo, et al., A hierarchically structured $Ni(OH)_2$ monolayer hollow-sphere array and its tunable optical properties over a large region, Advanced Functional Materials 17 (2007) 644–650.

[6] J.C. Jin, Y.Y. Wang, P. Liu, et al., An unusual independent 1D metal–organic nanotube with mesohelical structure and 1D–2D interdigitation, Crystal Growth & Design 10 (2010) 2029–2032.

[7] D. Yang, R. Wang, M. He, et al., Ribbon- and boardlike nanostructures of nickel hydroxide: synthesis, characterization, and electrochemical properties, Journal of Physical Chemistry B 109 (2005) 7654–7658.

[8] Y. Wang, J. Zhu, X. Yang, et al., Preparation of NiO nanoparticles and their catalytic activity in the thermal decomposition of ammonium perchlorate, Thermochimica Acta 437 (2005) 106–109.

[9] G. Mattei, P. Mazzoldi, M.L. Post, et al., Cookie-like Au/NiO nanoparticles with optical gas-sensing properties, Advanced Materials 19 (2007) 561–564.

[10] S.H. Lin, F.R. Chen, J.J. Kai, Electrochromic properties of nanocomposite nickel oxide film, Applied Surface Science 254 (2008) 3357–3363.

[11] X. Wang, J. Song, L. Gao, et al., Optical and electrochemical properties of nanosized NiO via thermal decomposition of nickel oxalate nanofibres, Nanotechnology 16 (2005) 37–40.

[12] H. Sato, T. Minami, S. Takata, et al., Transparent conducting p-type NiO thin films prepared by magnetron sputtering, Thin Solid Films 236 (1993) 27–31.

[13] J.K. Chang, M.T. Lee, C.H. Huang, et al., Physicochemical properties and electrochemical behavior of binary manganese–cobalt oxide electrodes for supercapacitor applications, Materials Chemistry and Physics 108 (2008) 124–131.

[14] X.M. Liu, X.G. Zhang, S.Y. Fu, Preparation of urchinlike NiO nanostructures and their electrochemical capacitive behaviors, Materials Research Bulletin 41 (2006) 620–627.

[15] J. He, H. Lindstrom, A. Hagfeldt, et al., Dye-sensitized nanostructured p-type nickel oxide film as a photocathode for a solar cell, Journal of Physical Chemistry B 103 (1999) 8940–8943.

[16] L. Xiang, X.Y. Deng, Y. Jin, Experimental study on synthesis of NiO nano-particles, Scripta Materialia 47 (2002) 219–224.

[17] T.L. Lai, Y.L. Lai, J.W. Yu, et al., Microwave-assisted hydrothermal synthesis of coralloid nanostructured nickel hydroxide hydrate and thermal conversion to nickel oxide, Materials Research Bulletin 44 (2009) 2040–2044.

[18] A.S. Vanetsev, V.K. Ivanov, Yu.V. Kolenko, et al., Synthesis of spherical oxide particles in microwave hydrolysis of Zr(IV), Ce(IV), and Ni(II) salt solutions, Doklady Chemistry 385 (2002) 175–177.

[19] L. Xu, Y. Ding, C. Chen, et al., 3D flowerlike α-nickel hydroxide with enhanced electrochemical activity synthesized by microwave-assisted hydrothermal method, Chemistry of Materials 20 (2008) 308–316.

[20] O. Garbuzenko, Y. Barenholz, A. Priev, Effect of grafted PEG on liposome size and on compressibility and packing of lipid bilayer, Chemistry and Physics of Lipids 135 (2005) 117–129.

[21] D.E. Eastman, J.L. Freeouf, Photoemission partial state densities of overlapping p and d states for NiO, CoO, FeO, MnO, and $Cr_2O_3$, Physical Review Letters 34 (1975) 395–398.

[22] G. Boschloo, A. Hagfeldt, Spectroelectrochemistry of nanostructured NiO, Journal of Physical Chemistry B 105 (2001) 3039–3044.

[23] T. Tsuboi, W. Kleemann, Fine structure of near infrared optical absorption in NiO, Journal of Physics: Condensed Matter 6 (1994) 8625–8628.

[24] A.J. Varkey, A.F. Fort, Solution growth technique for deposition of nickel oxide thin films, Thin Solid Films 235 (1993) 47–50.